The influence of the cloud shell on tracer budget measurements of LES cloud entrainment

Jordan T Dawe * and Philip H Austin

Department of Earth and Ocean Sciences, University of British Columbia, Vancouver, BC, Canada.

* *Corresponding author address:* Jordan T Dawe, Department of Earth and Ocean Sciences, University of British Columbia, 6339 Stores Road, Vancouver, BC, V6T 1Z4, Canada.

E-mail: jdawe@eos.ubc.ca

ABSTRACT

Direct measurements of rates of entrainment into and detrainment from cumulus cloud cores obtained from LES model cloud fields produce values twice as large as those produced from total water budget calculations. This difference can be explained by three effects: the presence of a shell of moist air around the cloud cores and drier air at the edge of the cloud core, the tendency for the mean tracer values of the entrained fluid to be greater than the mean tracer value of the cloud shell, and numerical errors in the calculation of the tracer budget. Preferential entrainment of shell air that is moving upward faster than the mean shell creates strong vertical momentum fluxes into the cumulus cloud core, making the assumption that cumulus clouds entrain fluid with zero vertical momentum incorrect. Variability in the properties of the moist cloud shell has strong impacts on entrainment values inferred from tracer budget calculations. These results indicate the dynamics of the cloud shell should be included in parametrization of cumulus clouds used in general circulation models.

1. Introduction

The rate at which air is entrained into and detrained from cumulus clouds affects cloud properties, cloud top height, and vertical transports of heat and moisture. Proper simulation of cumulus sub-grid scale fluxes in General Circulation Models (GCM) depends on the accurate parametrization of entrainment of environmental tracer properties into the clouds and detrainment of cloud properties into the environment (Bechtold et al. 2008; de Rooy and Siebesma 2010).

Entrainment and Detrainment may be defined mathematically as

$$E = -\frac{1}{A}\oint_{\hat{\mathbf{n}}\cdot(\mathbf{u}-\mathbf{u_i})<0} \rho\hat{\mathbf{n}}\cdot(\mathbf{u}-\mathbf{u_i})dl \tag{1a}$$

$$D = \frac{1}{A}\oint_{\hat{\mathbf{n}}\cdot(\mathbf{u}-\mathbf{u_i})>0} \rho\hat{\mathbf{n}}\cdot(\mathbf{u}-\mathbf{u_i})dl \tag{1b}$$

where E and D are the entrainment and detrainment rates in kg m^{-3} s^{-1}, ρ is the density of air in kg m^{-3} s^{-1}, $\mathbf{u}$ is the velocity of the air in m s^{-1}, $\mathbf{u_i}$ is the velocity of the cloud surface in m s^{-1}, A is the area of the cloud in m^2, $\hat{\mathbf{n}}$ is a unit vector directed out the cloud surface, and the path integral is taken around the cloud surface at a constant vertical level (Siebesma 1998). Entrainment and detrainment are thus caused by differences between the motion of the cloud surface and the motion of the air. This includes not just mixing processes, but also adiabatic processes such as condensation of fluid at cloud base. Many parameterizations use cloud core as the region over which to consider entrainment and detrainment, defined as regions having condensed liquid water, positive buoyancy, and upward vertical velocity. In this case, the motion of the cloud core surface is simply substituted for the motion of the cloud surface in equations (1).

Entrainment and detrainment rates impact GCM parametrizations in several ways. First, profiles of cloud vertical mass flux are usually calculated from parametrized entrainment values using the continuity equation for a simple entraining plume to represent an ensemble of cumulus clouds:

$$\rho\frac{\partial a}{\partial t} + \frac{\partial M_{core}}{\partial z} = E - D. \tag{2}$$

Here a is the fractional cloud core area and M_{core} is vertical cloud core mass flux (kg m^{-2} s^{-1}).

The level where the mass flux profile goes to zero then defines the location of the cloud ensemble top. This mass flux profile is combined with the entrainment rate of environmental air into the cloud and the detrainment rate of cloud air into the envrionment to generate vertical profiles of cloud water vapor, condensate, and temperature, and these profiles are then used to calculate the moistening of the environment by detrainment of cloud fluid (Tiedtke 1989; Kain and Fritsch 1990). Precipitation rates are also generated from the mass flux and tracer profiles produced from the entrainment and detrainment profiles. The wide range of effects that the entrainment and detrainment have make entrainment rate one of the strongest controls on the climate sensitivity of GCMs (Stainforth et al. 2005; Rougier et al. 2009).

Large Eddy Simulation (LES) is the primary tool used to study cloud entrainment and detrainment rates. LES mass entrainment and detrainment rates are typically obtained using budgets of conserved tracer variables to infer the amount of fluid exchange between the cloud ensemble and the surrounding air. Siebesma and Cuijpers (1995) derive the following equations for entrainment and detrainment of mass from the ensemble of cloud core plumes:

$$E_{\phi S}(\phi_{core} - \phi_{env}) = -M_{core}\frac{\partial \phi_{core}}{\partial z} - \frac{\partial \rho a \overline{w'\phi'}^{core}}{\partial z} - \rho a \frac{\partial \phi_{core}}{\partial t} + a\rho \left(\frac{\partial \bar{\phi}}{\partial t}\right)_{forcing} \tag{3a}$$

and

$$D_{\phi S}(\phi_{core} - \phi_{env}) = -M_{core}\frac{\partial \phi_{env}}{\partial z} + \frac{\partial \rho (1-a) \overline{w'\phi'}^{env}}{\partial z} + \rho(1-a)\frac{\partial \phi_{env}}{\partial t} - \rho(1-a)\left(\frac{\partial \bar{\phi}}{\partial t}\right)_{forcing} \tag{3b}$$

Where ϕ (with units denoted by $[\phi]$) represents any conserved tracer, such as the total specific humidity q_t (kg water kg^{-1} moist air) or the liquid-water moist static energy h (J kg^{-1}); w

is vertical velocity (m s^{-1}); *env* and *core* sub-and super-scripts denote horizontally averaged values conditionally sampled in the cloud environment and core; $forcing$ refers to tracer sources and sinks, such as radiation or subsidence, not included in the other terms; primed values represent anomalies relative to the horizontal mean; overbars represent horizontal averaging; and $E_{\phi S}(z)$ and $D_{\phi S}(z)$ are the total mass entrainment into and detrainment from the cloud core inferred from the tracer budget, in kg s^{-1} m^{-3}. We use the S subscript to differentiate E and D calculated via the Siebesma tracer budget method from other measures of mass exchanges, and we shall refer to values calculated by this method as "Siebesma tracer budget" entrainment and detrainment. For convenience, the various tracer and entrainment/detrainment rate subscripts used below are summarized in the Appendix.

Alternatively, entrainment and detrainment of mass can be calculated directly from the LES velocity and tracer fields. Romps (2010) recently presented a technique to measure local (grid scale) mass entrainment $e(x, y, z)$ and detrainment $d(x, y, z)$. Summing these point measurements horizontally gives $E_d(z)$ and $D_d(z)$, the total mass entrained into and detrained from the cloud core field in kg s^{-1} m^{-3}, where the d subscript indicates these quantities were calculated directly from the model velocity and tracer fields. His equation (2) is:

$$e - d = \frac{\partial}{\partial t}(\mathcal{A}\rho) + \nabla \cdot (\rho \mathbf{u} \mathcal{A}) \tag{4}$$

Here $\mathcal{A}$ is the "activity" of the fluid, where $\mathcal{A}$ is one at cloud core points and zero otherwise. The values of $e-d$ are averaged over the time that a grid cell experiences mass fluxes between an active and an inactive point, then positive $e-d$ values are considered to be purely e, and negative values, d. As noted above, we shall refer to entrainment and detrainment values

calculated by this method as "direct" E and D and denote them with the subscript d.

Romps found that such direct calculation of the entrainment and detrainment mass fluxes produced values roughly twice as large as the Siebesma tracer budget calculations. Romps attributed this difference to the Siebesma tracer budget calculation assumption that fluid exchanged between clouds and environment has the mean properties of the cloud or environment at that level, respectively. Studies of the dense, descending shell of moist air that forms around trade-wind cumulus clouds (Jonas 1990; Rodts et al. 2003; Heus and Jonker 2008; Jonker et al. 2008; Heus et al. 2009; Wang and Geerts 2010) suggest that the cloud shell properties are quite different than the core or environment properties, bolstering Romps' hypothesis. Since fluid exchanges between clouds and environment must pass through this shell, it is likely that it plays an important role in entrainment and detrainment dynamics.

Below we examine the sources of the discrepancy in entrainment and detrainment values calculated via tracer budgets and directly using (4). We show that the discrepancy is explained by three effects: the presence of the shell of moist air around the cloud cores and drier air at the edge of the cloud core, preferential entrainment of shell air with higher average humidity and upward velocity than the mean shell proterties which enhances tracer fluxes between the clouds and the environment, and errors in the calculation of the tracer budget. We derive a relation to transform the "direct" entrainment flux values into "Siebesma tracer budget" values suitable for use in one-dimensional simple entraining plume cloud parametrizations, and then use these transformed fluxes to evaluate the impact of the shell on tracer budget entrainment and detrainment rates of specific humidity and vertical velocity. Finally, we examine the dynamics that drives the preferential entrainment of air with

higher than average specific humidity and vertical velocity.

2. Model description

All LES calculations in this paper were made using the System for Atmospheric Modeling (SAM; Khairoutdinov and Randall 2003). Two model runs were performed, configured as standard Global Energy and Water Cycle Experiment (GEWEX) Cloud System Studies (GCSS; Randall et al. 2003) experiments: a Barbados Oceanographic and Meteorological Experiment (BOMEX; Siebesma et al. 2003) run, and an Atmospheric Radiation Measurement Study (ARM; Brown et al. 2002) run. The BOMEX run was performed on a 6.4 km x 6.4 km horizontal x 3.2 km vertical domain with 25 meter grid size in all directions for 6 hours, and the first three hours of simulation were discarded. The ARM run was performed on a 7.68 km x 7.68 km x 4.5 km domain with 30 meter grid size. Precipitation was disabled in both runs.

We have implemented the entrainment calculation scheme of Romps (2010) in SAM, allowing us to calculate the mass of air entrained into and detrained from cloud core directly from model ρ, $\mathbf{u}$, and $\mathcal{A}$. Romps (2010, eq. 4) also presents a method for calculating local entrainment and detrainment rates for any model variable in the same framework as (4), but neglects forcing and diffusion terms. These terms are significant for quantities like vertical momentum, so we modify Romps' equation to include their effects:

$$e\phi - d\phi = \frac{\partial}{\partial t}(\phi\mathcal{A}\rho) + \nabla\cdot(\phi\rho\mathbf{u}\mathcal{A}) - \rho\mathcal{A}S_\phi. \tag{5}$$

where S_ϕ is any non-advective source or sink term for ϕ, such as precipitation for q_t or

pressure gradient for w, in units of $[\phi]$ s^{-1}. The inclusion of these source/sink terms allows us to expand the definition of ϕ to include non-conserved fluid properties.

As with equation (4), the local $(e\phi)(x, y, z)$ and $(d\phi)(x, y, z)$ must be horizontally summed to give the total entrainment into or detrainment out of the cloud ensemble for any fluid property, but since ϕ can be negative for properties like vertical velocity, it is possible for entrainment to reduce and for detrainment to increase the various properties of the cloud core. To accommodate this effect, if the average value of ϕ is positive over the time that a grid cell experiences mass fluxes between an active and an inactive grid cell, then positive $e\phi - d\phi$ values are considered to be purely $e\phi$, and negative values, $d\phi$. However, if the average of ϕ is negative, then positive $e\phi - d\phi$ values are considered to be purely $(d\phi)(x, y, z)$, and negative values, $(e\phi)(x, y, z)$.

The obvious way to calculate the average value of ϕ is to perform a flux-weighted calculation, so that $\phi = (e\phi - d\phi)/(e - d)$. However, doing so for positive definite quantities, such as q_t, sometimes results in negative ϕ. The see the reason for this, consider a situation where $(e - d)$ integrated over the period of activity is found to be slightly bigger than zero for a grid cell. The Romps algorithm would assign E to a small value and D to be zero, but in reality the problem is unconstrained; as long as $E \approx D$, the net flux measured by the algorithm would be satisfied. At the same time, $Eq_t - Dq_t$ is found to be negative, due to E and D having similar magnitues but the detraining q_t being larger than the entraining q_t. In this case, $(Eq_t - Dq_t)/(E - D)$ will be negative, even though q_t is always positive. To avoid this problem, we calculate ϕ as a simple time average for the purpose of determining if $e\phi - d\phi$ is assigned to $e\phi$ or to $d\phi$. Horizontal summation of $(e\phi)$ and $(d\phi)$ then gives $(E\phi)_d(z)$ and $(D\phi)_d(z)$, the total entrainment and detrainment of a property for the cloud

ensemble in units of $[\phi]$ kg s^{-1} m^{-3} calculated directly from the model velocity and property fields.

3. Relationship Between Direct and Tracer Budget Entrainment

Romps (2010) established that the direct estimate of mass entrainment and detrainment yields values roughly twice the size of those calculated via conserved tracer budgets. Furthermore, examination of the ratios of the Siebesma mass entrainment and detrainment calculated via a total specific water budget (E_{qS}, D_{qS}) to the directly calculated values (E_d, D_d) over the diurnal cycle of an ARM LES reveals significant changes over the course of the day (Fig. 1). Thus, the tracer and direct measurements of E and D are not only significantly different, but have differing dynamics, which may need to be be accounted for in large-scale parametrizations that account for entrainment and detrainment. In this section we examine the sources of disagreement between direct and Siebesma tracer budget estimates of mass entrainment into and detrainment from the cloud core. We first consider the different assumptions about tracer values in the cloud core and environment, then look at relationships between entrainment/detrainment and tracer values and the different numerical approximations made in the Siebesma tracer budget and direct calculations.

a. E and D Cloud Shell Correction

Romps attributed the differences between ($E_{\phi S}$, $D_{\phi S}$) and (E_d, D_d) to the assumption made by Siebesma and Cuijpers (1995) that fluid entrained or detrained has the properties of the mean environment or cloud core, respectively. The fact that the mean core and environment properties are not representative of entraining and detraining fluid is shown in Fig. 2a. If we examine the horizontal mean specific humidity of the fluid at the "cloud core edge" (cloud core model grid cells that are nearest-neighbor adjacent to non-core cells), which presumably is the fluid being detrained, we see it is drier than the mean core. Similarly, the fluid just outside the cloud core in the "cloud core shell" (non-core model grid cells that are nearest-neighbor adjacent to core cells) which is available for entrainment is moister than the mean environment.

Budget equations that explicitly distinguish between the the moist cloud shell and dry cloud edge allow us to transform (E_d, D_d) values into equivalent Siebesma tracer budget values $(E_{\phi S}, D_{\phi S})$ and back again. We start our derivation with the observation that both the tracer budget and direct value of E and D are consistent with the continuity equation (equations 2 and 4). This implies that

$$E_\phi - D_\phi = E_d - D_d. \tag{6}$$

Similarily, the entrainment and detrainment rates of water must be consistent with the total water budget, giving us

$$E_\phi \phi_{env} - D_\phi \phi_{core} = E_d \phi_E - D_d \phi_D. \tag{7}$$

Combining these equations and solving for E_ϕ and D_ϕ in turn results in:

$$E_{\phi T} = E_d - \left[E_d \frac{(\phi_E - \phi_{env})}{(\phi_{core} - \phi_{env})} + D_d \frac{(\phi_{core} - \phi_D)}{(\phi_{core} - \phi_{env})} \right] \tag{8a}$$

$$D_{\phi T} = D_d - \left[E_d \frac{(\phi_E - \phi_{env})}{(\phi_{core} - \phi_{env})} + D_d \frac{(\phi_{core} - \phi_D)}{(\phi_{core} - \phi_{env})} \right]. \tag{8b}$$

Here we have added the T subscript to the $E_{\phi T}$ and $D_{\phi T}$ terms to denote that these values are equivalent to Siebesma tracer budget values, but have been calculated by transforming the direct entrainment and detrainment values. We shall refer to these values as "transformed" entrainment and detrainment. The bracketed terms represent the bias introduced by assuming that entrained/detrained air has the properties of the mean environment and core. Thus, to convert from (E_d,D_d) to ($E_{\phi T}$, $D_{\phi T}$), both E_d and D_d must be reduced by $E_d A + D_d B$, where $A = (\phi_E - \phi_{env})/(\phi_{core} - \phi_{env})$ and $B = (\phi_{core} - \phi_D)/(\phi_{core} - \phi_{env})$.

Note that rearrangement of A gives $\phi_E = A\phi_{core} + (1 - A)\phi_{env}$, meaning that A can be thought of as the fraction of mean core air in a mixture of mean core and mean environment air needed to produce the properties of the entrained fluid. Similarily, $\phi_D = B\phi_{env} + (1 - B)\phi_{core}$ and B can be thought of as the fraction of mean environment air in a mixture of mean core and mean environment air needed to produce the properties of the detrained fluid. Since the fluid being entrained or detrained does not neccessarily originate at the level it is entrained or detrained at, we cannot assume that a fraction A of the entrained air is modified core air. Nevertheless, A and B are likely related to the recirculation of entrained and detrained air.

Alternatively, we can solve for E_d and D_d, arriving at

$$E_{dT} = E_{\phi S} + \left[E_{\phi S} \frac{(\phi_E - \phi_{env})}{(\phi_D - \phi_E)} + D_{\phi S} \frac{(\phi_{core} - \phi_D)}{(\phi_D - \phi_E)} \right]. \tag{9a}$$

$$D_{dT} = D_{\phi S} + \left[E_{\phi S} \frac{(\phi_E - \phi_{env})}{(\phi_D - \phi_E)} + D_{\phi S} \frac{(\phi_{core} - \phi_D)}{(\phi_D - \phi_E)} \right]. \tag{9b}$$

In this case, to convert from ($E_{\phi S}$, $D_{\phi S}$) to (E_{dT}, D_{dT}), both $E_{\phi S}$ and $D_{\phi S}$ must be increased by $E_{\phi S}a + D_{\phi S}b$, where $a = (\phi_E - \phi_{env})/(\phi_D - \phi_E)$ and $b = (\phi_{core} - \phi_D)/(\phi_D - \phi_E)$. Note that under both these transformations $E_d - D_d = E_\phi - D_\phi$, preserving mass continuity, and furthermore, $E_d A + D_d B = E_\phi a + D_\phi b$.

We now have relationships allowing us to transform the unbiased E_d and D_d values into biased Siebesma tracer budget $E_{\phi S}$ and $D_{\phi S}$ values, which are better suited for simple entraining plume parametrization of cloud fields. Comparison of E_{qS} and D_{qS} ($E_{\phi S}$ and $D_{\phi S}$ inferred using total specific moisture q_t as the tracer) with E_d and D_d shows the direct entrainment and detrainment magnitudes are significantly larger than the Siebesma tracer budget values (Figure 2b and 2c, grey and dotted lines). Using (8) to calculate E_{qT} and D_{qT} with $q_E = q_{edge}$, the horizontal mean humidity in the cloud edge, and $q_D = q_{shell}$, the horizontal mean humidity in the cloud shell, results in values quite close to the Siebesma tracer budget values above the middle of the cloud layer. The transformation also duplicates the negative detrainment values near cloud base that are typically produced by tracer calculations.

b. Preferential Entrainment of Moist, Ascending Air

Relative to the Siebesma tracer budget values, the transformed E_{qT} and D_{qT} values calculated using $q_E = q_{edge}$ and $q_D = q_{shell}$ are still too large near cloud base. We can partially explain the difference between the transformed mass entrainment/detrainment values and the Siebesma tracer budget values as being the result of the mean tracer values of the entrained

and detrained air being different than the mean value of the shell and edge air, respectively. Using the mean shell and edge values of tracers to transform the direct entrainment and detrainment assumes that any fluid parcel in the shell or edge is equally likely to be entrained or detrained. In reality, mixing relatively dry air into the cloud core is more likely to cause evaporation, which will drive detrainment, while mixing relatively moist air into the cloud core is more likely to produce a saturated fluid mixture, resulting in entrainment. This suggests that the moistest shell parcels are more likely to undergo entrainment than the average shell parcel, and the driest edge parcels are more likely to detrain than the average edge parcel.

We can directly calculate the effective tracer value at which entrainment occurs by taking the total tracer entrainment $(E\phi)_d$ calculated via equation (5) and dividing it by the total mass entrainment E_d so that $\phi_{entrain} = (E\phi)_d/E_d$. Similarly, the effective tracer value at which detrainment occurs can be found from $\phi_{detrain} = (D\phi)_d/D_d$. Examination of these values from the BOMEX simulation using q_t for ϕ shows $q_{entrain}$ is moister than q_{shell} (Figure 3a), indicating entrainment occurs preferentially at the moistest parts of the shell. Conversely, there is little difference between between $q_{detrain}$ and q_{edge}, indicating the detrained parcels tend to have the mean moisture of the cloud core edge.

Using $q_{entrain}$ and $q_{detrain}$ to transform E_d and D_d results in smaller E_{qT} and D_{qT} values than utilizing the mean shell and edge properties (solid black line, Fig. 3b and 3c). E_{qT} calculated using $q_E = q_{entrain}$ and $q_D = q_{detrain}$ is about half the magnitude of the Siebesma tracer budget entrainment value throughout the cloud layer. This new transformation reduces the large entrainment and detrainment values near cloud base, which improves the overall shape of the fluxes. Above mid-cloud, however, there is less correspondence between

transformed E_{qT} and D_{qT} values and the Siebesma tracer budget values E_{qS} and D_{qS} when compared to the shell and edge correction of Figure 3.

c. Numerical Errors

An additional source of discrepancy between the Siebesma tracer budget and the Romps direct calculation is numerical truncation errors due to the differing advection schemes used by each calculation. Changing the advection scheme in the Romps direct calculation from a first-order upwind scheme to a second-order MPDATA scheme results in changes in E_d and D_d of up to 40% (Dawe and Austin 2011). The Siebesma tracer budget calculated using (3) accounts for the vertical advection of tracer properties by taking derivatives of mean vertical tracer profiles, along with averaged vertical Reynolds fluxes. The differences in the numerics between these calculations and the fully three dimensional MPDATA advection algorithm used by SAM means the results will not be exactly the same.

Normally these types of errors are not overwhleming, but the form of the equations (8), which transform a direct entrainment estimate into an equivalent tracer budget entrainment, serve to amplify numerical truncation errors in the Romps direct calculation. This can be better seen by using an alternate form of the transformation from direct to equivalent tracer budget values presented by Romps (2010, equations (11) and (12)):

$$E_{\phi T}(\phi_{core} - \phi_{env}) = \phi_{core}(E_d - D_d) - ((E\phi)_d - (D\phi)_d) \tag{10a}$$

$$D_{\phi T}(\phi_{core} - \phi_{env}) = \phi_{env}(E_d - D_d) - ((E\phi)_d - (D\phi)_d) \tag{10b}$$

Both (3) and (10) estimate $E_\phi(\phi_{core} - \phi_{env})$ and $D_\phi(\phi_{core} - \phi_{env})$, but the Romps estimate relies on taking the differences $(E_d - D_d)$ and $((E\phi)_d - (D\phi)_d)$, both of which are between

large quantities that have nearly identical magnitudes, which tends to magnify numerical errors present in each individual term. Furthermore, these two difference terms are then differenced again, amplifying the numerical errors a second time.

This effect can be seen by comparing the values of $\phi_{core}(E-D)$ and $((E\phi)-(D\phi))$ that are estimated via (3a) and (10a). First, we must identify which terms in (3a) correspond to $\phi_{core}(E-D)$ and which to $((E\phi)-(D\phi))$. The first correspondence can be found by multipling equation (2) by ϕ_{core}:

$$\phi_{core}(E-D) = \phi_{core}\left(\rho\frac{\partial a}{\partial t} + \frac{\partial M_{core}}{\partial z}\right). \tag{11}$$

Combining this with equations (3a) and (10a), we find

$$(E\phi)-(D\phi) = \rho\frac{\partial(a\phi_{core})}{\partial t} + \frac{\partial(M_{core}\phi_{core})}{\partial z} + \frac{\partial\rho a\overline{w'\phi'}^{core}}{\partial z} - a\rho\left(\frac{\partial\bar{\phi}}{\partial t}\right)_{forcing}. \tag{12}$$

Comparing the Romps and Siebesma $\phi_{core}(E-D)$ values (Fig. 4a) calculated using total specific water q_t as the budget tracer, shows that the Romps value (calculated via $q_{core}(E_d - D_d)$) agrees well with the Siebesma value calculated using (11). Similarily, the Romps $(E\phi)-(D\phi)$ values (Fig. 4b) calculated using $(Eq)_d - (Dq)_d$ are quite similar to the the Siebesma values calulated using (12). However, when the difference of these terms is taken (Fig. 4c), the similar magnitudes of $\phi_{core}(E-D)$ and $(E\phi)-(D\phi)$ causes the result to be dominated by numerical errors. The order 5% differences in the estimates of $\phi_{core}(E-D)$ and $(E\phi)-(D\phi)$ combine to result in a factor of two difference between Siebesma tracer budget and the Romps tracer budget.

The neglect of turbulent diffusion in the Siebesma bulk tracer calculation is one last possible source of discrepency between E_{qT} and E_{qS} . This is easily checked by neglecting

turbulent diffusion in the $\rho\mathcal{A}S_\phi$ term of equation (5); doing so results in a change of only TK% in the value of E_{qT} (not shown), not nearly enough to explain the discrepancy.

4. E_q, E_h and E_w Differences

Equations (8a) or (8b) imply that the Siebesma tracer budget method will measure different entrainment and detrainment values for fluid properties with differing values of $A = (\phi_E - \phi_{env})/(\phi_{core} - \phi_{env})$ and $B = (\phi_{core} - \phi_D)/(\phi_{core} - \phi_{env})$. With this in mind we compare transformed $E_{\phi T}$ and $D_{\phi T}$ values produced by liquid water moist static energy h and vertical velocity w with those produced using total specific moisture q_t.

Liquid water moist static energy shows a similar relative distribution of core, edge, shell, environment, entrained, and detrained properties when compared to q_t, indicating a tight coupling between these variables in the cloud dynamics. Because these properties are so tightly coupled, the transformed E_{hT} and D_{hT} values are nearly identical to the E_{qT} and D_{qT} (not shown).

Vertical velocity shows very different relative profiles compared to q_t or h (c.f. Fig. 5a and Fig. 3a). There is a much wider spread in the w values, with the shell having nearly zero vertical velocity and the edge being halfway between the core and the environment. $w_{detrain}$ is slightly larger than the value of w in the cloud core edge, while $w_{entrain}$ is much larger than w in the shell, becoming roughly the same value as w_{edge}. Since $w_{entrain}$ and $w_{detrain}$ are both larger than w_{shell} and w_{edge} this implies that rapidly rising air is both preferentially entrained and detrained over slowly rising air. These effective entrainment and detrainment w values produce E_{wT} and D_{wT} (solid black line, Fig. 5c and Fig. 5c) that are quite different than the

transformed entrainment and detrainment produced by q_t and h (dotted line, Fig. 5b and 5c); E_{wT} is negative over the whole of the cloud field, and D_{wT} is half the magnitude of D_{qT} over much of the cloud layer.

Finally, we examine the temporal variability of $A = (\phi_E - \phi_{env})/(\phi_{core} - \phi_{env})$ and $B = (\phi_{core} - \phi_D)/(\phi_{core} - \phi_{env})$ from the transformation equations (8a) and (8b) in the ARM model run. Since A represents the fraction of core air in a mixture of core and environmental air which has the properties of ϕ_E, and B represents the fraction of environmental air in a mixture of core and environmental air which has the properties of ϕ_D, A and B provide information about the amount of recirculation of entrained and detrained fluid occuring at different model heights. However, A and B cannot be considered exact mixing fractions, as the source heights of air mixtures may be different than the height at which they entrain or detrain, and not all mixtures of core and environment properties are equally likely to undergo entrainment.

A and B calculated for q_t both show strong changes over the ARM diurnal cycle (Figure 6, a and b). Near cloud base, A is nearly one while B is nearly zero, implying that both the entrained and detrained air have the properties of the cloud core air. This is due to the main entrainment process at cloud base being condensation of rising thermals instead of mixing; buoyant updrafts simply condense without modification of their properties. Similarily, the air that detrains from the clouds at cloud base is almost undiluted because most entrainment at this level comes from the well-mixed sub-cloud layer below and so has properties nearly identical to the cloud core. At cloud top, A is also nearly one while B is nearly zero, implying that both the entrained and detrained air have the properties of the cloud core air. Here, this is due to the main detrainment process from the core being clouds becoming negatively

buoyant as θ_v in the inversion increases faster than heating due to condensation can add buoyancy to the cloud core (Wu et al. 2009). Since this process does not depend on mixing, the air detraining from the core is relatively undiluted by the environment. Conversely, much of the air surrounding the remaining cloud core which is available for entrainment was previously detrained from the core without mixing, and so has the properties of the core air.

As the clouds mix into the inversion over the course of the day, they cause the inversion to rise. This means that points in the mid-cloud layer are less influenced by the adiabatic entrainment and detrainment processes occuring at cloud base and cloud top, and so the effects of mixing become more prominent. By the end of the day, A within the cloud layer has values near 0.6, suggesting that a significant amount of re-entrainment of air previously detrained from the core still occurs. B has values near 0.2, indicating that air detraining from the core is relatively undiluted by environmental air; this is sensible, since relatively little dilution by environmental air is required to cause the core air to become neutrally buoyant and detrain.

When calculated for w on the other hand, A reaches a value around 0.4 and B goes to 0.6. The difference between these values and the values of A and B calculated for q_t is the result of buoyancy and pressure gradient forces on the mixtures, and the stronger tendency for upward-moving shell parcels to be entrained relative to the tendency to entrain moister shell parcels. In other words, a relatively dry, rapidly ascending shell parcel is more likely to be entrained than a relatively moist, slowly ascending shell parcel. This is especially apparent near cloud base where the values of A are larger than 1, due to the mean entrained parcels having a larger upward velocity than the mean core parcels.

Performing these calculations with fixed values of $(\phi_{core} - \phi_{env})$, to remove changes due

to movement of the mean environment and core profiles, shows similar results. Changes in the properties of the entraining and detraining fluid due to the dynamics of mixing and entrainment in the shell clearly are active in determining the rates at which properties entrain and detrain.

5. Causes of Preferential Entrainment of Moist, Ascending Air

The reason that shell air which is moister and ascending faster than the mean shell is more likely to be entrained can be seen by comparing instantaneous snapshots of the model values of local mass entrainment e, moisture entrainment eq_t, and vertical velocity entrainment ew. Since the Romps (2010) method of calculating e and d requires taking time averages, it is unsuitable for calculating instantaneous entrainment fields. Instead, we use an alternative method we have devised that substitutes spatial interpolation for time averaging (Dawe and Austin 2011). This alternative method results in slightly smaller values of e and d than those produced by Romps' method, but the two calculations show good agreement in variability. The eq_t and ew fields are calculated simply by multiplying the value of e by the values of q_t and w, respectively.

Comparing the e, eq_t, and ew fields shows that e and eq_t have a very similar spatial pattern, but ew is concentrated in regions where strong updrafts enter the cloud core (Figure 7). The reason for this can been seen by examining the buoyancy, condensed liquid water, and vertical velocity fields that define the cloud core. Of these three fields, buoyancy is the

strongest constraint determining if air is part of the core. However, regions exist far above cloud base where air has become negatively buoyant but maintains upward velocity and condensed liquid water. As this air continues to rise more condensation occurs, which heats the updraft, makes it positively buoyant, and thus entrains it into the core. In this way, entrainment is positively correlated with both q_t and w. This process occurs fairly often in our model cloud field, as evidenced both by our manual examination of the output fields, and the size of the difference between w_{shell} and $w_{entrain}$ in the mean profiles.

6. Discussion

Considering all these results, we now turn to the most important question of all: which entrainment value is the right one? The unsatisfying answer is that it depends on the purpose for which the entrainment is to be used.

Consider a cumulus cloud parametrization based upon a simplified form of the continuity equation which assumes the cloud fraction is constant,

$$\frac{\partial M_{core}}{\partial z} = E - D \tag{13}$$

a cloud budget equation that assumes mean vertical advection is balanced by entrainment of mean environmental properties,

$$M_{core}\frac{\partial \phi_{core}}{\partial z} = E(\phi_{env} - \phi_{core}) \tag{14}$$

and a simple detrainment forcing equation,

$$\rho\frac{\partial \phi_{env}}{\partial t} = D(\phi_{core} - \phi_{env}). \tag{15}$$

ϕ_{env} is input to the parametrization from the GCM. If we assume we have a perfect parametrization of M_{core} and ϕ_{core} at cloud base with which to construct mean core mass flux and tracer profiles, we wish the E and D values to produce a profile of $\partial\phi_{core}/\partial t$ to force the GCM which agrees with LES results for a similar mean environmental profile. The E and D we desire then is closer to $E_{\phi S}$ and $D_{\phi S}$ than E_d and D_d, but nevertheless must be modified to account for the time tendency and Reynolds flux budget terms we have neglected. This also implies that we should have different $E_{\phi S}$ and $D_{\phi S}$ values for properties with different distribution patterns around the clouds.

Using values near E_d and D_d instead would require modifying equation (14) to

$$M_{core}\frac{\partial\phi_{core}}{\partial z} = E(\phi_{core} - \phi_E) - D(\phi_{core} - \phi_D) \tag{16}$$

and equation (15) into

$$\rho\frac{\partial\phi_{env}}{\partial t} = D(\phi_D - \phi_{env}) - E(\phi_E - \phi_{env}). \tag{17}$$

Now, instead of calculating different E and D values for each tracer we wish to model, we must instead calculate ϕ_E and ϕ_D values for each property that is entrained or detrained. While it is possible this would produce a better parametrization, it seems simpler to fold the effects of ϕ_E and ϕ_D into the E and D values and keep the equations in their less complex form.

On the other hand, the true values of the mass entrainment and detrainment are important for comparison of LES results with field studies, or possibly for calculations of aerosol reactions whose chemical properties are dependent on the concentration of liquid water in the air (Hoppel et al. 1994). They are also vital for diagnosing mass exchanges of individual

clouds in an LES ensemble, for which a simple "environment" and "cloud core" mean tracer budget may be difficult to define.

The large positive value of $w_{entrain}$ is clearly inconsistent with the often-made assumption that fluid entrained into the cloud core has negligible vertical momentum (Simpson and Wiggert 1969; Gregory 2001; Siebesma et al. 2003). This is reflected in the negative magnitude for the transformed E_{wT} shown in Fig. 5b and the smaller value of D_{wT} compared with D_{qT} in Fig. 5c: since w_{env} is slightly negative, the transformed velocity entrainment must be negative to bring positive velocity into the core. The negative w entrainment values (and the large negative detrainment values produced near cloud base for both q_t and w) emphasize the artificial nature of the Siebesma tracer budget entrainment and detrainment. The Siebesma entrainment and detrainment values are mathematical quantities that satisfy both the continuity equation (2) and the tracer budget of the cloud core under the assumption that the core entrains mean environment fluid and detrains mean cloud core fluid.

While the tendency for rapidly ascending shell air to be entrained more often than the slower parts of the shell was found for cloud core entrainment, we would like to emphasize that this process is not an artifact of the cloud core sampling; similar results appear when we perform entrainment calculations for simple cloudy regions (areas of condensed liquid water). In this case, vertical advection of air can drive condensation, converting environment air into cloud air, and thus driving entrainment of air into the cloud.

As both BOMEX and ARM model runs involved non-precipitating shallow cumulus, we have ignored the effects of precipitation. Precipitation is generally not considered part of the turbulent mixing processes associated with entrainment and detrainment in parametrization, instead being represented by a sink term in the liquid water budget (Tiedtke 1989; Kain and

Fritsch 1990). Nevertheless, incorporating precipitation into the Siebesma tracer budget and direct entrainment calculations would be relatively simple. The precipitation flux divergence rate would be a new sink/source forcing term in Siebesma's equation (3), and would be part of the forcing term $\rho \mathcal{A} S_\phi$ in Romps' equation (5), resulting in precipitation flux divergence not being counted as part of the detrainment. Specifying the advection terms would be somewhat trickier since, depending on the complexity of the microphysics scheme, moisture might be advected as a single q_t field or advected as separate hydrometeor classes. However, this would simply mean adding extra advection terms for each hydrometeor class. Once these effects were properly incorporated into the calculations, the transformations between (E_d, D_d) and (E_{qT}, D_{qT}) would be unchanged.

7. Conclusion

We have explained the differences between values of entrainment and detrainment of mass calculated via tracer budgets and direct flux calculations by taking into account the properties of the cloud shell, the tendency for the mean tracer values of the entrained fluid to be greater than the mean tracer value of the cloud shell, and differences in the numerical methods used by the two calculations. Furthermore, the tendency for the moistest, fastest-rising regions of the shell to be entrained more often than the drier, slower parts appears to be the result of upward advection of negatively buoyant, saturated air so that condensation causes latent heating, making the air buoyant and entraining it into the core. These effects suggest that the dynamics of the moist cloud shell have a significant role in mediating fluxes between the clouds and the environment.

Direct entrainment and detrainment calculations should be used to help improve our understanding of the dynamics of cloud mass exchanges and radial variation in cloud properties, with an eye to folding these effects into the simplest cloud parametrization possible. This should include using the behavior of various tracers to produce different E and D values for q_t and h than for w, and possibly other cloud properties as well. Doing so has the potential to improve GCM parametrization of the magnitude and variability of mass and tracer exchanges between clouds and their environment.

Acknowledgments.

Support for this work was provided by the Canadian Foundation for Climate and Atmospheric Science through the Cloud Aerosol Feedback and Climate network. We thank Marat Khairoutdinov for making SAM available to the cloud modeling community. We would also like to thank David Romps and two anonymous reviewers whose comments significantly improved the quality of this paper. All figures were generated using the matplotlib library in the Python programming language.

APPENDIX

Table of Notation

Table 1 goes here.

REFERENCES

Bechtold, P., M. Koehler, T. Jung, F. Doblas-reyes, M. Leutbecher, M. J. Rodwell, F. Vitart, and G. Balsamo, 2008: Advances in simulating atmospheric variability with the ECMWF model: From synoptic to decadal time-scales. *Q. J. R. Meteorol. Soc.*, **134 (634, Part A)**, 1337–1351, doi:10.1002/qj.289.

Brown, A. R., et al., 2002: Large-eddy simulation of the diurnal cycle of shallow cumulus convection over land. *Q. J. R. Meteorol. Soc.*, **128**, 1075–1093.

Dawe, J. T. and P. H. Austin, 2011: Interpolation of LES cloud surfaces for use in direct calculations of entrainment and detrainment, submitted to Monthly Weather Review.

de Rooy, W. C. and A. P. Siebesma, 2010: Analytical expressions for entrainment and detrainment in cumulus convection. *Q. J. R. Meteorol. Soc.*, **136 (650)**, 1216–1227, doi: 10.1002/qj.640.

Gregory, D., 2001: Estimation of entrainment rate in simple models of convective clouds. *Q. J. R. Meteorol. Soc.*, **127 (571, Part A)**, 53–72.

Heus, T. and H. J. J. Jonker, 2008: Subsiding shells around shallow cumulus clouds. *J. Atmos. Sci.*, **65**, 1003–1018.

Heus, T., C. F. J. Pols, H. J. J. Jonker, H. E. A. V. den Akker, and D. H. Lenschow, 2009: Observational validation of the compensating mass flux through the shell around cumulus clouds. *Q. J. R. Meteorol. Soc.*, **135**, 101–112.

Hoppel, W. A., G. M. Frick, J. Fitzgerald, and R. E. Larson, 1994: Marine boundary-layer measurements of new particle formation and the effects nonprecipitating clouds have on aerosol-size distribution. *J. Geophys. Res.-Atmos.*, **99**, 14 443–14 459.

Jonas, P. R., 1990: Observations of cumulus cloud entrainment. *Atmos. Res.*, **25**, 105–127.

Jonker, H. J. J., T. Heus, and P. P. Sullivan, 2008: A refined view of vertical mass transport by cumulus convection. *Geophys. Res. Let.*, **35**, L07 810.

Kain, J. S. and J. M. Fritsch, 1990: A one-dimensional entraining/detraining plume model and its application in convective parameterization. *J. Atmos. Sci.*, **47**, 2784–2802.

Khairoutdinov, M. F. and D. A. Randall, 2003: Cloud resolving modeling of the arm summer 1997 iop: model formulation, results, uncertainties, and sensitivities. *J. Atmos. Sci.*, **60**, 607–625.

Randall, D., et al., 2003: Confronting models with data: The GEWEX cloud systems study. *Bulletin of the American Meteorological Society*, **84 (4)**, 455–469, doi:10.1175/BAMS-84-4-455, URL `http://journals.ametsoc.org/doi/abs/10.1175/BAMS-84-4-455`, `http://journals.ametsoc.org/doi/pdf/10.1175/BAMS-84-4-455`.

Rodts, S. M. A., P. G. Duynkerke, and H. J. J. Jonker, 2003: Size distributions and dynamical properties of shallow cumulus clouds from aircraft observations and satellite data. *J. Atmos. Sci.*, **60**, 1895–1912.

Romps, D. M., 2010: A direct measure of entrainment. *J. Atmos. Sci.*, **67 (6)**, 1908–1927.

Rougier, J., D. M. H. Sexton, J. M. Murphy, and D. Stainforth, 2009: Analyzing the climate sensitivity of the HADSM3 climate model using ensembles from different but related experiments. *J. Climate*, **22 (13)**, 3540–3557, doi:10.1175/2008JCLI2533.1.

Siebesma, A. P., 1998: Shallow cumulus convection. *Buoyant Convection in Geophysical Flows*, E. J. Plate, Ed., Kluwer Academic Publishers, 441–486.

Siebesma, A. P. and J. W. M. Cuijpers, 1995: Evaluation of parametric assumptions for shallow cumulus convection. *J. Atmos. Sci.*, **52**, 650–666.

Siebesma, A. P., et al., 2003: A large eddy simulation intercomparison study of shallow cumulus convection. *J. Atmos. Sci.*, **60 (10)**, 1201–1219.

Simpson, J. and V. Wiggert, 1969: Models of precipitating cumulus towers. *Mon. Wea. Rev.*, **97 (7)**, 471.

Stainforth, D. A., et al., 2005: Uncertainty in predictions of the climate response to rising levels of greenhouse gases. *Nature*, **433**, 403–406.

Tiedtke, M., 1989: A comprehensive mass flux scheme for cumulus parameterization in large-scale models. *Mon. Wea. Rev.*, **117**, 1779–1800.

Wang, Y. and B. Geerts, 2010: Humidity variations across the edge of trade wind cumuli: Observations and dynamical implications. *Atmos. Res.*, **97 (1-2)**, 144 – 156, doi:DOI: 10.1016/j.atmosres.2010.03.017.

Wu, C.-M., B. Stevens, and A. Arakawa, 2009: What controls the transition from shallow to deep convection? *J. Atmos. Sci.*, **66**, 1793–1806.

List of Tables

TABLE 1. List of Symbols

Symbol	Units	Definition	First Occurrence
E, D	kg m^{-3} s^{-1}	Cloud core mass entrainment/detrainment rate	(2)
$E_{\phi S}$, $D_{\phi S}$	kg m^{-3} s^{-1}	Mass entrainment/detrainment rate calculated using Siebesma tracer budget	(3a), (3b)
e, d	kg m^{-3} s^{-1}	Local mass entrainment/detrainment rate	(4)
E_d, D_d	kg m^{-3} s^{-1}	Cloud core mass entrainment/detrainment rate calculated directly from model velocity and tracer fields	§1
$e\phi$, $d\phi$	$[\phi]$ kg m^{-3} s^{-1}	Local cloud core ϕ entrainment/detrainment rate	(5)
$(E\phi)_d$, $(D\phi)_d$	$[\phi]$ kg m^{-3} s^{-1}	Cloud core ϕ entrainment/detrainment rate calculated directly from model velocity and tracer fields	§2
$E_{\phi T}$, $D_{\phi T}$	kg m^{-3} s^{-1}	Cloud core mass entrainment/detrainment rate calculated by transforming a directly calculated value into an equivalent tracer budget value	(8a), (8b)
E_{dT}, D_{dT}	kg m^{-3} s^{-1}	Cloud core mass entrainment/detrainment rate calculated by transforming a tracer budget value into an equivalent directly calculated value	(9a), (9b)
ϕ	$[\phi]$	Any fluid tracer, such as q_t (kg kg^{-1}), h (J kg^{-1}), or w (m s^{-1})	§1
ϕ_{core}	$[\phi]$	Mean cloud core ϕ	§3a
ϕ_{edge}	$[\phi]$	Mean cloud edge ϕ	§3a
ϕ_{shell}	$[\phi]$	Mean cloud shell ϕ	§3a
ϕ_{env}	$[\phi]$	Mean environment ϕ	§3a
$\phi_{entrain}$	$[\phi]$	Effective value of ϕ being entrained calculated from direct entrainment	§3b
$\phi_{detrain}$	$[\phi]$	Effective value of ϕ being detrained calculated from direct detrainment	§3b
ϕ_E	$[\phi]$	Placeholder for the value of ϕ assumed to be entraining	(8a)
ϕ_D	$[\phi]$	Placeholder for the value of ϕ assumed to be detraining	(8b)

List of Figures

4 Sizes of: a) $\phi_{core}(E-D)$ calculated with total specific humidity q_t using Romps direct entrainment/detrainment ($q_{core}[E_d - D_d]$, black line) and Siebesma tracer budget entrainment/detrainment ($q_{core}(\rho\partial a/\partial t+\partial M_{core}/\partial z)$); b) $(E\phi)-(D\phi)$ calculated using Romps direct entrainment/detrainment $((Eq)_d-(Dq)_d$, black line) and Siebesma tracer budget ($\rho\partial(aq_{core})/\partial t + \partial(M_{core}q_{core})/\partial z + \partial(\rho a\overline{w'q'}^{core})/\partial z - a\rho(\partial\bar{q}/\partial t)_{forcing}$, grey line); and c) the difference of a) and b), $\phi_{core}(E - D) - ((E\phi) - (D\phi))$, for the direct entrainment/detrainment (black lines) and the Siebesma tracer budget entrainment/detrainment (grey lines). Note how small relative differences in the values of a) and b) result in large relative differences in c). 36

5 Result of transforming direct entrainment values into equivalent w budget values. a) Mean profiles of the effective w values being entrained (black line), and detrained (dotted line), overlaid on the mean w values of the core, edge, shell and environment. These w values are used to transform directly calculated values of b) entrainment and c) detrainment (grey line) into equivalent tracer budget values (black line). The entrainment and detrainment values transformed using q_t are shown for comparison (dotted lines). 37

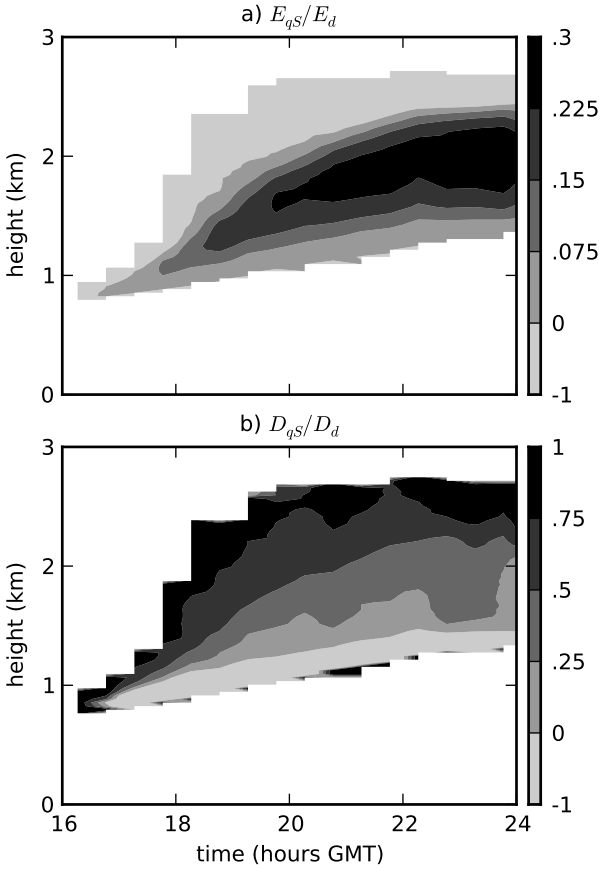

FIG. 1. Ratio of the Siebesma specific humidity tracer budget a) entrainment and b) detrainment values to the directly calculated values over the duration of the ARM model run.

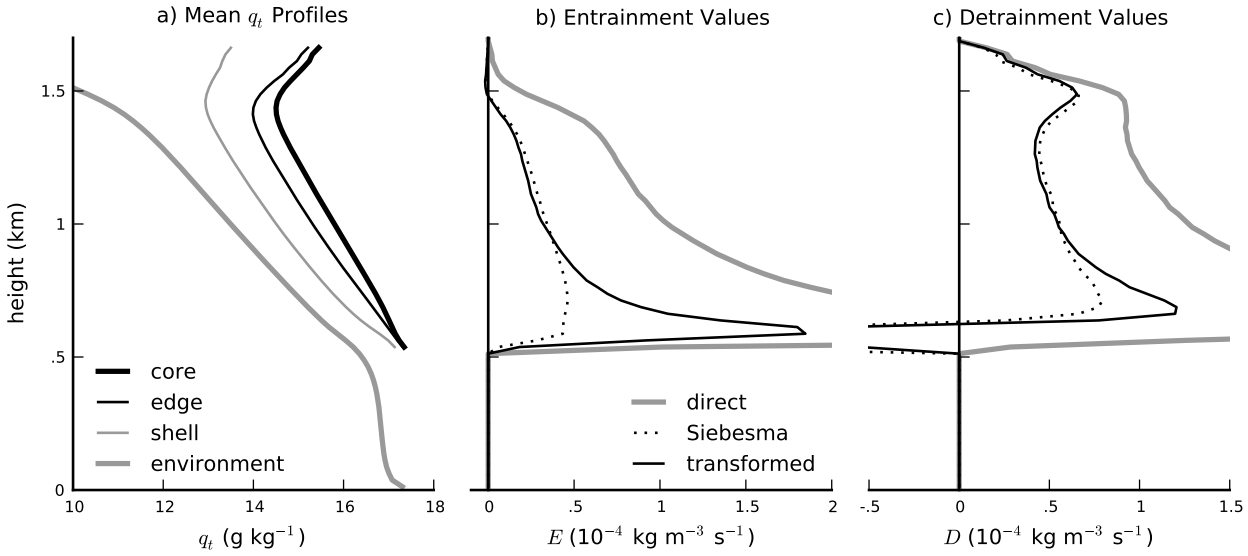

FIG. 2. Result of transforming direct entrainment values into equivalent tracer budget values using mean cloud core shell and edge properties. a) Mean profiles of the total specific humidity in the cloud core (thick black line), cloud core edge (thin black line), cloud core shell (thin grey line), and cloud core environment (thick grey line). These q_t values are used to transform directly calculated values of b) entrainment and c) detrainment (grey line) into equivalent tracer budget values (black line). The Siebesma tracer budget entrainment and detrainment are shown for comparison (dotted lines).

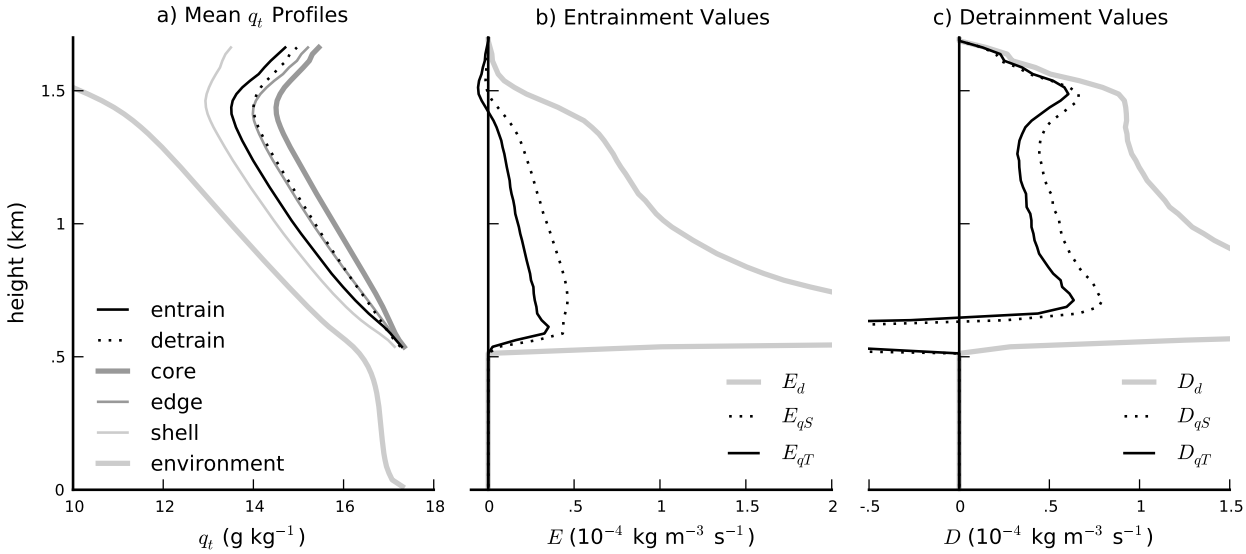

FIG. 3. Result of transforming direct entrainment values into equivalent tracer budget values using effective entrainment and detrainment properties. a) Mean profiles of the effective total specific humidity values being entrained ($q_{entrain}$, black line), and detrained ($q_{detrain}$ dotted line), overlaid on the mean total specific humidity values of the core, edge, shell and environment. These q_t values are used to transform directly calculated values of b) entrainment and c) detrainment (grey line) into equivalent tracer budget values (black line). The Siebesma tracer budget entrainment and detrainment are shown for comparison (dotted lines).

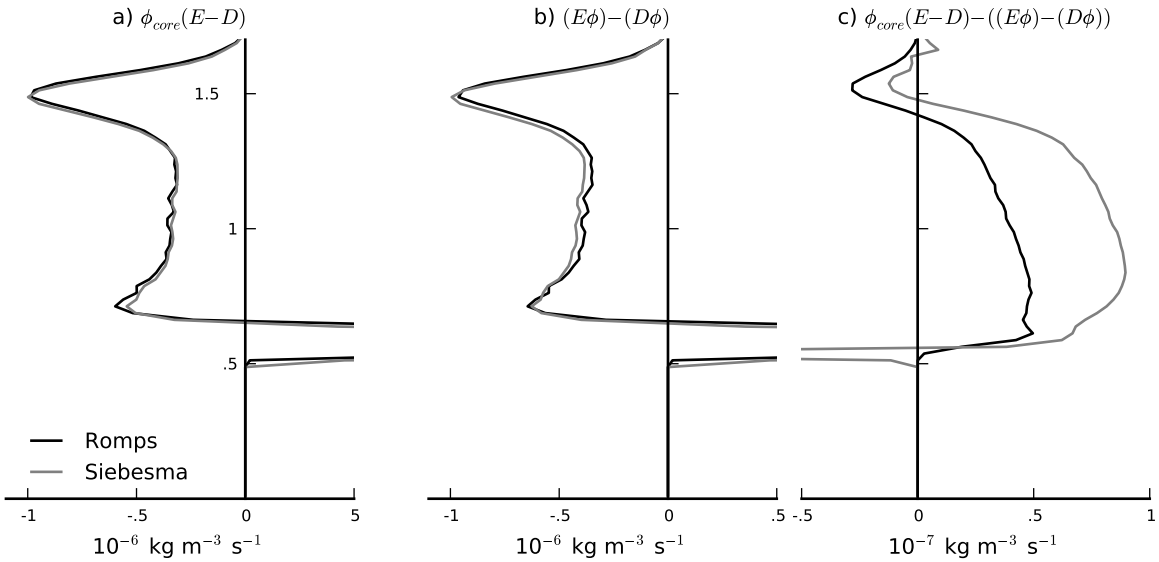

FIG. 4. Sizes of: a) $\phi_{core}(E-D)$ calculated with total specific humidity q_t using Romps direct entrainment/detrainment ($q_{core}[E_d - D_d]$, black line) and Siebesma tracer budget entrainment/detrainment ($q_{core}(\rho\partial a/\partial t + \partial M_{core}/\partial z)$); b) $(E\phi)-(D\phi)$ calculated using Romps direct entrainment/detrainment ($(Eq)_d - (Dq)_d$, black line) and Siebesma tracer budget ($\rho\partial(aq_{core})/\partial t + \partial(M_{core}q_{core})/\partial z + \partial(\rho a\overline{w'q'}^{core})/\partial z - a\rho(\partial\bar{q}/\partial t)_{forcing}$, grey line); and c) the difference of a) and b), $\phi_{core}(E-D)-((E\phi)-(D\phi))$, for the direct entrainment/detrainment (black lines) and the Siebesma tracer budget entrainment/detrainment (grey lines). Note how small relative differences in the values of a) and b) result in large relative differences in c).

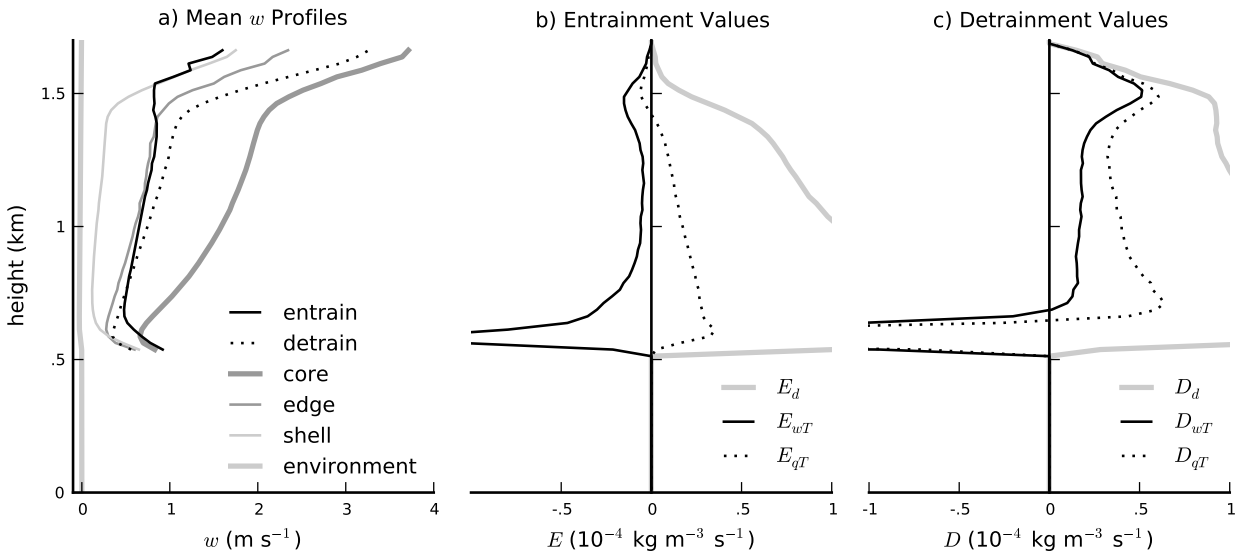

FIG. 5. Result of transforming direct entrainment values into equivalent w budget values. a) Mean profiles of the effective w values being entrained (black line), and detrained (dotted line), overlaid on the mean w values of the core, edge, shell and environment. These w values are used to transform directly calculated values of b) entrainment and c) detrainment (grey line) into equivalent tracer budget values (black line). The entrainment and detrainment values transformed using q_t are shown for comparison (dotted lines).

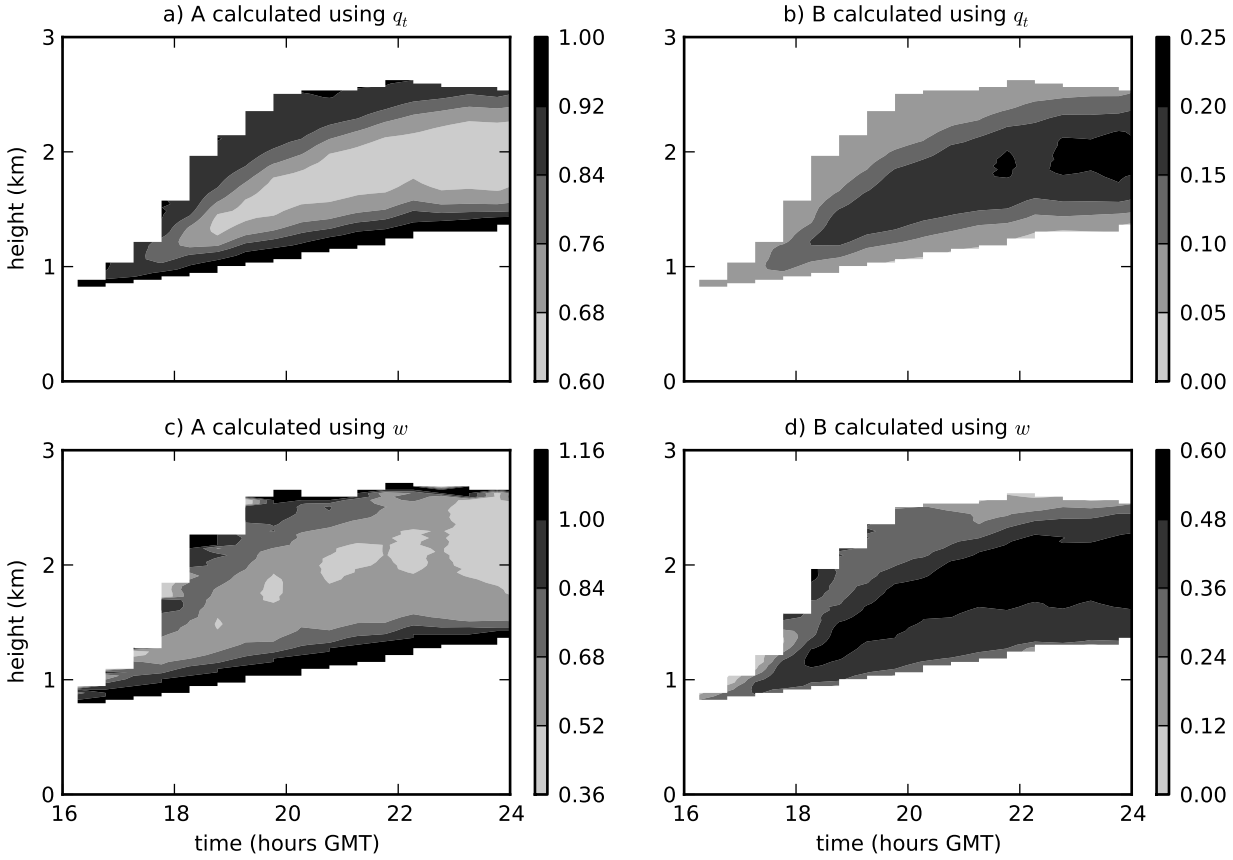

FIG. 6. Variation in a) the fraction of core air in a mixure of core and environmenal air needed to produce the mean humidity entrained by the clouds, b) the fraction of environmental air in a mixure of core and environmenal air needed to produce the mean humidity detrained by the clouds, c) the fraction of core air in a mixure of core and environmenal air needed to produce the mean vertical velocity entrained by the clouds, and d) the fraction of environmental air in a mixure of core and environmenal air needed to produce the mean vertical velocity detrained by the clouds, over the duration of the ARM model run.

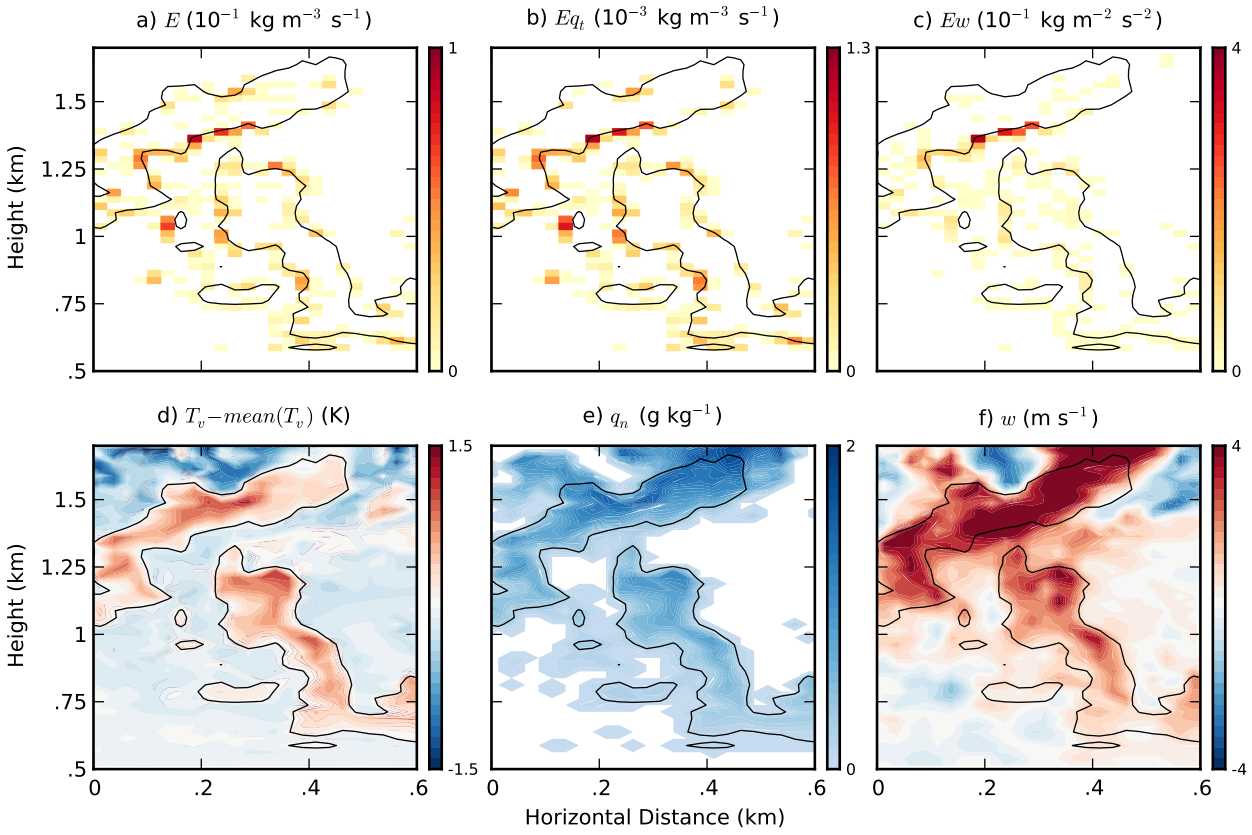

FIG. 7. Instantaneous vertical cross-section of directly calculated cloud core mass entrainment (a), humidity entrainment (b), vertical velocity entrainment (c), buoyancy (d), condensed liquid water (e), and vertical velocity (f) of a single model cloud, illustrating the tendency to entrain shell air that is rising faster than the mean shell. Black lines indicate the edge of the cloud core in each figure.